

Prior based Sampling for Adaptive LiDAR

Amit Shomer
Tel Aviv University
amitshomer@gmail.com

Shai Avidan
Tel Aviv University
avidan@eng.tau.ac.il

Abstract

We propose *SampleDepth*, a Convolutional Neural Network (CNN), that is suited for an adaptive LiDAR. Typically, LiDAR sampling strategy is pre-defined, constant and independent of the observed scene. Instead of letting a LiDAR sample the scene in this agnostic fashion, *SampleDepth* determines, adaptively, where it is best to sample the current frame. To do that, *SampleDepth* uses depth samples from previous time steps to predict a sampling mask for the current frame. Crucially, *SampleDepth* is trained to optimize the performance of a depth completion downstream task. *SampleDepth* is evaluated on two different depth completion networks and two LiDAR datasets, KITTI Depth Completion and the newly introduced synthetic dataset, SHIFT. We show that *SampleDepth* is effective and suitable for different depth completion downstream tasks. Our code is publicly available¹.

1. Introduction

LiDAR is shaping to be an important ingredient in autonomous vehicles, as well as other AR/VR applications. As such, it is of interests to make it as efficient as possible.

There are several types of LiDAR and here we focus on scanning LiDARs, where the LiDAR scans the scene in order to measure the distance to different points in the 3D environment. The sampling pattern of LiDARs today is based on the hardware constraints of the device itself and are agnostic to the 3D scene. In this setting, the LiDAR produces a sparse set of depth measurements and extensive literature evolved over the years to develop depth completion algorithms [35, 19, 24, 25]. These algorithms take the sparse depth map and the corresponding RGB image captured by a camera, to produce a dense depth map.

Clearly, increasing the number of depth samples will improve the reconstructed depth map. On the downside, it will prolong acquisition time and increase hardware cost. We wish to find a better sampling pattern that will achieve bet-

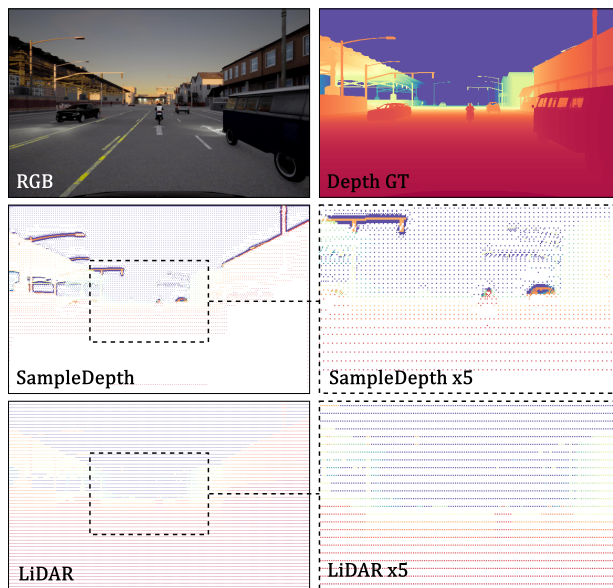


Figure 1. **Prior based sampling.** Our solution uses information from previous time steps as priors in order to predict the the position of the adaptive LiDAR sample mask for the current frame.

ter depth completion results with the same sampling budget.

Towards this end, we consider three scenarios. The first, that serves as a baseline, is the *agnostic* sampling pattern that is in use today. In this setting, the sampling does not adapt to the scene. The second is a *fixed* sampling pattern that is based on learning a fixed sampling mask for the entire training set. For example, learning an optimal mask on a large collection of videos collected by a driving vehicle. The last is an *adaptive* sampling mask that is based on previous samples. This is the focus of this work. Figure 1 shows the difference between agnostic sampling and adaptive sampling.

Our workhorse is a novel network, termed *SampleDepth*, that uses depth maps from previous time steps to determine the current sampling mask. Crucially, *SampleDepth* is trained subject to a target depth completion network, so it can be used in conjunction with any such network. More-

¹<https://github.com/amitshomer/SampleDepth>

over, SampleDepth can be trained with one depth completion network and then used, as is, with another. The use of temporal data is a common practice in computer vision for a variety of tasks. However, to the best of our knowledge, we are the first to use it for adaptive LiDAR sampling.

We investigate two variants of the adaptive approach. In the first, we actually predict the current depth map from past measurements. In the second, we simply provide the past measurements and let the network implicitly learn from it.

We evaluate SampleDepth on two datasets, a real one and a simulated one, and find that it outperforms the existing agnostic sampling approach across a range of sampling rates. Furthermore, we show that SampleDepth can be used with different depth completion networks and, in fact, can be trained with one depth completion network and then used, as is, with another.

2. Related Work

Depth completion. The purpose of depth completion tasks is to take a sparse depth map and transform it into a dense depth map. Uhrig *et al.* [34] suggests using convolutional neural networks (CNN) to complete sparse laser scan data. Since then, many studies [4, 17, 1, 7] demonstrated that neural networks are capable of creating dense depth maps by taking only sparse LiDAR scans as an inputs. Other studies [24, 25, 3, 27, 35] used also an RGB images to guide the depth completion process.

Several studies have examined the effects of different depth map sparsity on the depth completion performance. Qiu *et al.* [27] uniformly sub-sample the raw LiDAR maps and checked the performance of their model against it. Karaman and Ma [24] randomly sampled the ground truth in order to increase robustness and increase training data size. Lu *et al.* [23] use only a single-line of the LiDAR and an RGB image to generate dense depth map.

Depth Sampling. Recent works investigated a variety of sampling techniques for 3D points. The sampling of those points is intended to optimize various tasks, including classification, segmentation or reconstruction for a given number of sampling points. Dovrat *et al.* [6] proposed a learned task-oriented simplification which process raw point clouds. Lang *et al.* [18] extended this work by approximating the sampling operation with a differentiable nearest neighbor operator.

A number of studies focused on sampling 3D points that are projected into 2D maps. These studies examined the possibility of obtaining better sampling patterns than what is achievable today with LiDAR hardware for the reconstruction task. To maximize the performance of disparity map reconstruction, Liu *et al.* [22] proposed a two-stage random sampling scheme. Wolf *et al.* [39] introduced an algorithm that uses super-pixels to divide the image plane,

and then sample each super-pixel. In another work, by Bergman *et al.* [2], a deep neural network was used to sample at very low sampling rates. Initially, they use grid sampling and then move those points to better locations using a vector flow fields.

Gofer *et al.* [11] use an ensemble of black-box predictors to determine the next point to sample. They do so by dynamically selecting the next point to sample within the current frame. Tcenov and Gilboa [33] extend that work. First, they construct an uncertainty map by using a neural network guided by RGB images. Then, they create the final sampled map using Gaussian sampling. In the sampled process, both Gofer *et al.* [11] and Tcenov [33] utilize an iterative approach.

Taguchi *et al.* [32] use iterative approach as well. Contrary to Gofer *et al.* [11], who create a new uncertainty map every iteration using the depth completion task, they create an uncertainty map only once. Afterwards, a neural network module is used to update it in every iteration.

Without exception, all the sampling methods mentioned above are not using prior past frames, as we do.

Video prediction is the task of inferring future video frames based on past frames. To address this issue, a number of approaches have been proposed. Some approaches [38, 14, 30, 37, 36] use recurrent neural networks (RNN) to make next frame prediction.

Transform inputs are another popular method for synthesizing frames. Liang *et al.* [20] proposed a generative adversarial network (GAN) with joint optical-flow. Jiang *et al.* [15] learned a model to predict offset vectors in order to interpolate frames. Liu *et al.* [21] expanded this method by creating a spatially-displaced convolution module. The module learned the new value and the displaced location for each pixel, and used that to synthesize a new image.

Simpler approaches use a CNN to predict the next frame. A modified U-Net [28] was used by Liu *et al.* [21] to predict the next frame and to detect anomalies. Gao *et al.* [9] achieved state-of-the-art results using CNNs trained with MSE loss.

3. Method

A depth completion network f takes an RGB image I and a sparse depth map D_S to create a dense depth map \hat{D} that is as similar to the ground truth depth map D as possible. The sampling pattern is governed by a sampling matrix M with $k = |M|$ samples. That is, $D_S = D \odot M$, where \odot denotes element-wise multiplication (i.e., the elements of M are either 0 or 1). Typically, M is the sampling pattern dictated by the LiDAR and is usually agnostic of the scene.

We wish to design a sampling network g , termed SampleDepth, that uses some prior \hat{D}^- on the scene to produce a better sampling mask M with the same number of samples

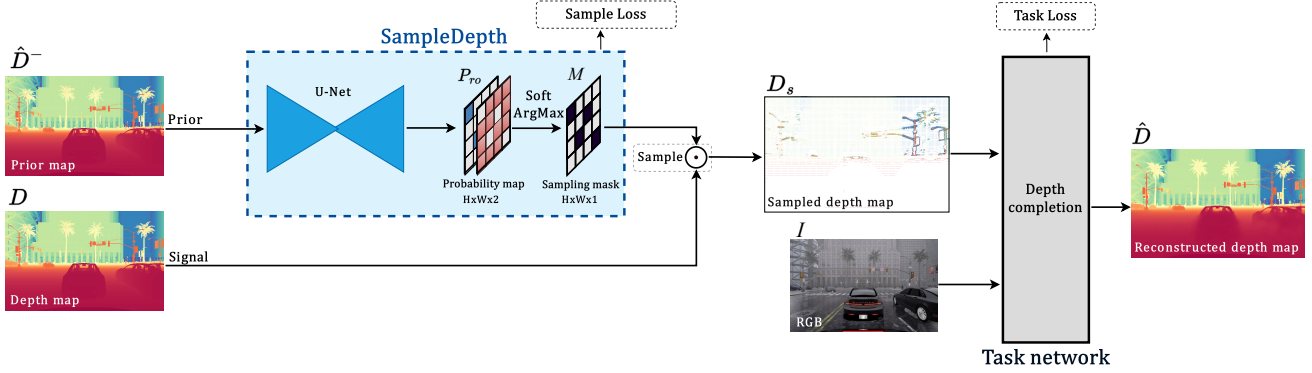


Figure 2. **The proposed SampleDepth sampling process.** The SampleDepth network takes the prior input and reproduces the sample mask as an output. In this example, the sampled signal and the prior are the same. In section 4.2 we explore additional configurations of priors and signals.

k :

$$M^* = \underset{M}{\operatorname{argmin}} \|f(D \odot g(\hat{D}^-), I) - D\|_2^2 \quad \text{s.t. } |M| = k \quad (1)$$

As proposed by Dai *et al.* [5], we use a simple yet efficient method for sampling 2D inputs. In essence, the principle involves creating a mask and then element-wise multiplying the input signal with it.

Figure 2 gives an overview of our proposed approach. First, the prior \hat{D}^- is given as input to $\mathbb{U}(\cdot)$, a convolution neural network (CNN) based on U-Net [28] architecture. The output of this network is a probability map, $P_{ro} \in \mathbb{R}^{H \times W \times 2}$. The channels of P_{ro} denote the probability of the pixels to be sampled. Next, by applying Soft-Argmax [8, 12], a differentiable operator, on the probability map P_{ro} , the sampling mask $M \in \mathbb{R}^{H \times W}$ is created. This mask is a close approximation of a binary mask. Finally, the sampling mask is multiplied, element-wise, with the ground truth depth map D , in order to obtain the sampled depth map D_S .

The basic training regime of SampleDepth consists of three steps. First, a depth completion task is pre-trained independently with an agnostically sampled signal input and an RGB image. Then, we freeze the weights of the task network. Next, SampleDepth takes the signal and samples it. The output of SampleDepth is then fed into the frozen task network. Finally, the task network and SampleDepth are fine-tuned together.

In order to train our model, we use the following loss terms:

$$L_{total} = L_{task}(D_s, I) + \alpha L_{sample}(M) \quad (2)$$

The first term, $L_{task}(D_s, I)$, optimizes the sampled depth map D_s to the task. It preserves the task performance with the sample depth map. $L_{sample}(M)$ is responsible to reduce the number of sampled points to the desired value. This can

be formulated as:

$$L_{sample}(M) = \frac{||M| - k|}{k} \quad (3)$$

Where k represents the desired number of sampled points.

3.1. An Adaptive Model

For applications such as adaptive LiDAR, we aim to sample the depth map D_t , at time t , given past reconstructed depth maps $\hat{D}_{t-1:t-b}^- \triangleq \{\hat{D}_{t-1}^-, \hat{D}_{t-2}^-, \dots, \hat{D}_{t-b}^-\}$, where $b \geq 1$. We evaluated two variants of an adaptive model:

PredNet. In this variant, an explicit prediction of the current reconstructed depth map, \hat{D}_t , is created based on past reconstructed maps, $\hat{D}_{t-1:t-b}$. The predicted reconstructed depth map, \hat{D}_t , serves as the prior to sample the real-world scene, i.e., the ground-truth (GT).

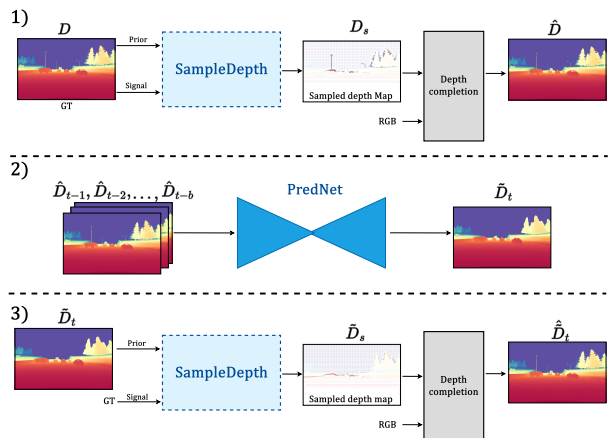


Figure 3. **Training regime of the proposed Adaptive Model.** This figure refers to the **PredNet** version. In the **ImplicitPred** model stage 2 is not performed. Instead, The previously constructed depth maps, $\hat{D}_{t-1:t-b}$, are directly fed into SampleDepth in stage 3.

The full training regime of the PredNet process is depicted in Figure 3. First, SampleDepth is trained with D , GT depth maps, which served both as a signal and as a prior. The reconstructed depth maps, \hat{D}_t , estimated during training, are saved. This will be used as the past reconstructed maps, $\hat{D}_{t-1:t-b}$, in the next step.

Next, in order to create the predicted reconstructed map, \tilde{D}_t , the past reconstructed maps, $\hat{D}_{t-1:t-b}$ are given as input to a U-Net based network (PredNet). The PredNet loss is an L_1 with respect to the GT.

Finally, the explicit prediction of the current reconstructed depth map, \tilde{D}_t , is being used as a prior to sampling the depth from the real-world scene.

ImplicitPred. This variant bypass the depth map reconstruction step altogether. Instead, past reconstructed depth maps, $\hat{D}_{t-1:t-b}$, are fed directly to SampleDepth as priors.

In this case, an additional loss term, $L_{SampledMaps}$ has been included. This loss term encourages the depth maps generated at this stage, \hat{D}_s , to be as close as possible to the sampled depth map, D_s , generated where GT serves as both the signal and the prior. For this purpose, L_1 loss is used.

3.2. An End-to-End Adaptive Model

We trained PredNet using $\hat{D}_{t-1:t-b}$, as described in subsection 3.1. But this data was created using GT priors, which is not available in reality. To provide a complete solution, we would like to remove this constraint. The reconstructed depths maps should be derived from previous iterations of the algorithm, in which the GT is not used as a prior. Our End-to-End solution is summarized in Algorithm 1.

Algorithm 1 End-to-End Adaptive Model

Inputs: Images $I_{1:T}$, Dense Depth Maps $D_{1:T}$, Memory size S , Number sampled points k
 $b \leftarrow S$
for $t \leftarrow 1$ to T **do**
 if $t < S$ **then**
 $D_s \leftarrow \text{SampleRandom}(D_t, k)$
 else
 $\tilde{D}_t \leftarrow \text{PredNet}(\hat{D}_{t-1:t-b})$
 $D_s \leftarrow \text{SampleDepth}_k(\tilde{D}_t) \odot D_t$
 end if
 $\hat{D}_t \leftarrow \text{DepthCompletion}(D_s, I_t)$
end for

To clarify, in the step in which SampleDepth is being used, the depth map, D_t , refers to the signal that is being sampled, and the reconstructed map, \tilde{D}_t , refers to the prior. In addition, SampleDepth_k refers to a network that was trained to sample k points.

4. Experiments

4.1. Datasets and Implementation Details

We conduct experiments on two datasets: KITTI Depth Completion [34][10] and SHIFT[31].

KITTI Depth Completion: The dataset provides both RGB images and aligned sparse depth maps generated by projecting 3D LiDAR points on the corresponding image frames. A sparse LiDAR map has about 5% valid pixels and a ground truth depth map has around 16% valid pixels. The dataset contains 86K frames for training, together with 7K validation frames and 1K test frames. The validation has a split of 1K subset frames, which is referred to as "selected validation set". Following Gansbeke *et al.* [35], for both training and testing, input images and depth maps were cropped to 256×1216 due to the lack of LiDAR points in the top part of the images.

SHIFT: is a synthetic dataset for autonomous driving. It is designed to provide highly diverse environmental conditions for real-world applications. We used the official discrete split that was released by the authors. A total of 3K training sequences and 500 validation sequences are included. Each sequence is composed of 51 frames, which are sampled at 1Hz. We have down-scaled the images to a size of 400×640 pixels.

Implementation Details. SampleDepth is implemented in PyTorch [26] and trained on four NVIDIA GTX 1080 Ti and evaluated using one GPU. As our depth completion baseline we used the network proposed by Gansbeke *et al.* [35]. Li *et al.* [19] depth completion network was also used for further ablation studies. A detailed description of the training regime can be found in the supplementary.

Evaluation Method. SampleDepth is trained to optimize a depth completion downstream task. Therefore, the proposed method is evaluated with respect to the quality of the reconstructed depth maps. As is common, we use the root mean square error (RMSE) as well as the mean absolute error (MAE).

SampleDepth is trained to produce a pre-defined number of sampling points. This works well with the SHIFT dataset because it is synthetic. That is, for every sampled pixel there is a corresponding depth value.

This is not the case in the KITTI dataset because the depth data is sparse. This is true even if we use the ground truth depth map provided in the KITTI dataset. In order to address this issue, we propose two approaches:

KITTI (sparse). We sample more pixels than is actually required and then use only pixels that actually have a depth value associated with them.

Pseudo KITTI (dense). As part of the pre-processing step, we trained Gansbeke *et al.* [35] to estimate a dense

Method	Sub-method	Prior	19K sampled points		4.8K sampled points
			SHIFT (dense)	Pseudo KITTI (dense)	KITTI (sparse)
Agnostic	-	-	3.158	0.825	0.787
SampleDepth	Fixed mask	Training set	2.974	0.681	0.672
	Adaptive (ImplicitPred)	Previous reconstructed depth maps	2.525	-	-
	Adaptive (PredNet)	Previous reconstructed depth maps	2.472	0.652	-
	Lower bound	Sampled signal(GT depth)	1.643	0.631	0.52

Table 1. **Comparison of different sampling methods on two datasets (SHIFT, KITTI).** In both datasets, the adaptive method outperforms the agnostic and fixed mask methods. The SHIFT dataset contains dense depth maps that have been sampled. Pseudo KITTI (dense) refers to the pseudo GT which was created and sampled. KITTI (sparse) denotes that the original GT has been sampled. See text for details. Results are reported in the form of RMSE[m].



Figure 4. **Fixed sampling mask.** Two examples of the fixed mask (red dots) on images from the datasets. The mask contains roughly 19K points. (Left) KITTI dataset. (Right) SHIFT dataset. In both cases, the majority of the sampling points is concentrated in the upper half of the mask. Objects in these areas are typically located at greater distances.

depth map by randomly selecting 20% points from the GT. These dense depth maps were saved and used for pseudo GT purposes.

Fixed mask. As a baseline above the *agnostic* method being used today, we compute a fixed mask. This method is intended to learn a single fixed sampling mask that is optimized for the entire data set. For this purpose, we use SampleDepth without any prior input. The U-Net encoder-decoder was removed and we initialized the probability map, P_{ro} , values with kaiming normal [13]. The *fixed* mask was then used as-is during inference to sample the GT.

Figure 4 shows the fixed sampling map for the KITTI and SHIFT datasets. As can be seen, the sampling pattern are not identical and exhibit the difference between the two datasets. We observe that a greater number of points are sampled from the upper half of the image for both datasets. Due to the automotive structure of the scene, the objects in these parts are typically located at a greater distance.

4.2. Results

Table 1 reports results of our method in different settings and on different datasets.

The top part of the table shows results of sampling 19K points in the SHIFT dataset. As can be seen, the agnostic approach achieves a depth completion RMSE of 3.158m. A fixed mask improves the error to 2.974m, while adaptive methods cut the error down to 2.472m. The "Lower bound"

row shows the error if we had access to the ground truth as a prior. In this case, the error is 1.643m.

ImplicitPred uses the previously reconstructed depth maps as a prior to predict where to sample. In PredNet, a predication of the current depth map is made first, and then serves as a prior to the sampling of the current time step depth map. We found that using the last four frames gave the best results for PredNet and the last two frames gave the best results for ImplicitPred.

The two adaptive methods are compared in Table 1 for 19K sampled points. The two methods yield very similar results, with PredNet performing slightly better. Compared with agnostic sampling, PredNet shows a significant improvement of 22%, while ImplicitPred gains 20% over agnostic sampling. Similar results can be observed in the KITTI dataset when using either the sparse depth maps, or the completed depth maps, as the ground truth to sample from. We conclude that adaptive sampling does indeed reduce the RMSE error of the reconstructed depth maps.

A quantitative comparison of sampled patterns between the Lower-bound and PredNet variants is presented in Figure 5. There is a tendency for both methods to sample fewer points in very close depth ranges. In the Lower-bound sampling pattern, there is a high concentration of sampling points near the edges. In PredNet, in certain cases, the edge patterns appear more blurry, while in other cases, some of the edge details have almost completely disappeared.

End-to-End Adaptive Model Putting all the pieces together, we evaluate the performance of the adaptive method on a longer sequences of 51 frames. We used agnostic sampling on the first four frames of each sequence. After that we used PredNet in order to predict the next reconstructed depth map. This prediction was used as a prior to sample the current time step GT by SampleDepth. The PredNet and SampleDepth networks were not trained or fine-tuned again for this experiment. Weights were taken from the stage described in subsection 3.1.

Figure 6 illustrates how well our end-to-end algorithm

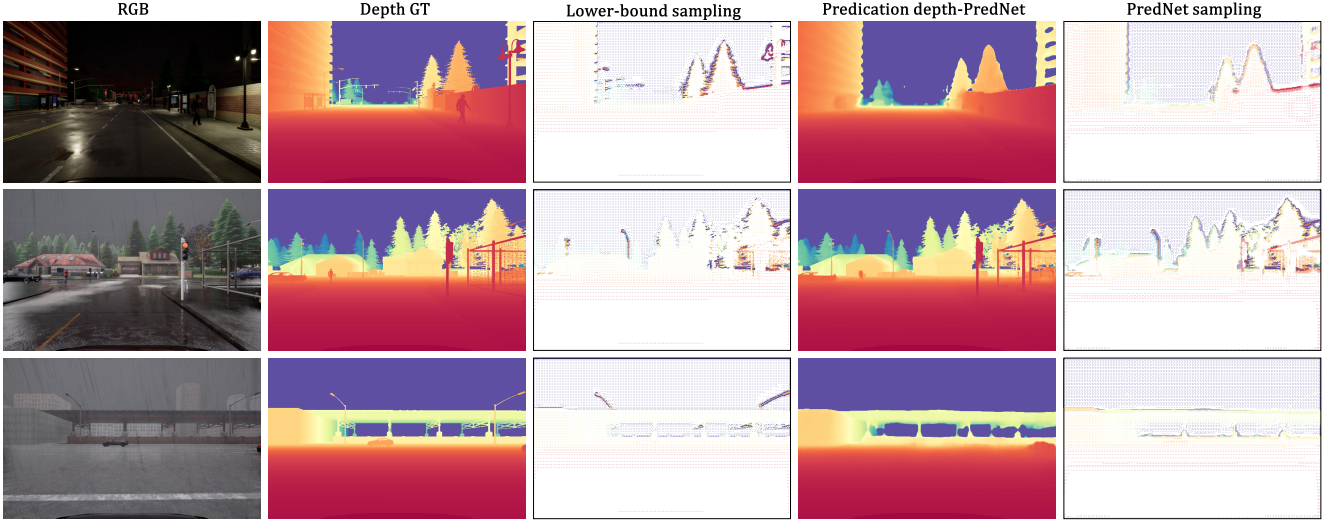


Figure 5. **Lower Bound vs PredNet sampling.** We compare two priors to sampling the GT. PredNet is using previous frames as prior. Lower Bound is a theoretical approach, where the GT itself is used as a prior. From left to right we show the input RGB image, the Depth GT that is to be sampled, the sampling mask based on the GT itself (this forms a lower-bound on sampling), the predicted depth map by our PredNet, and finally the PredNet based sampling mask. The sampling mask is less dense in regions where the prediction maps fails to predict fine details. For example, in the first and third rows, PredNet did not predict the traffic signs and light poles, therefore the correlated sample maps have a lower density in those regions.

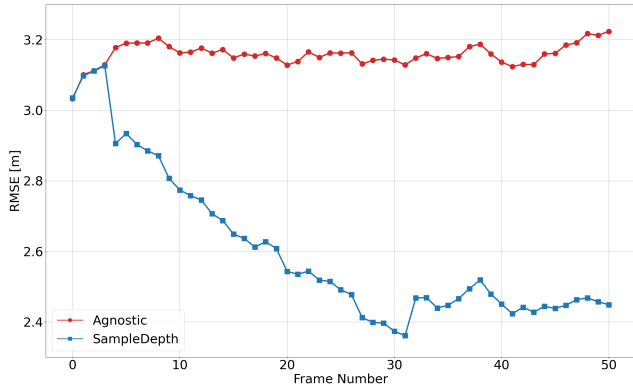


Figure 6. **SampleDepth End-to-End adaptive model solution mean accuracy per frame.** SHIFT discrete validation set has 500 different sequence of driving scenes. At 1Hz each sequence has 51 frames.

converges to the same range of accuracy values shown in Table 1. The solution remains stable over time and outperforms the agnostic sampling by approximately 25% in the steady state.

Comparison with the state-of-the-art The closest alternatives we could find in the literature are the work of Wolf *et al.* [39] and Gofer *et al.* [11] that represent the current state-of-the-art depth sampling on the KITTI Depth Completion dataset.

A fair comparison between these methods and ours is not possible, because they do not use prior depth maps and we

Method	4096		2048		1024		Inference time
	RMSE	MAE	RMSE	MAE	RMSE	MAE	
Super pixel sampler[39]	-	-	-	-	1.302	0.522	-
Adaptive LiDAR using Ensemble Variance[11]	0.750	0.230	0.900	0.298	1.077	0.473	1100ms (2x2080GTX)
SampleDepth (Fixed-mask)	0.747	0.245	0.959	0.304	1.140	0.420	17ms (1x1080Ti)
SampleDepth (Lower-bound)	0.534	0.181	0.567	0.237	0.751	0.334	
SampleDepth(PredNet) (Pseudo KITTI)	1.116	0.425	1.692	0.918	-	-	-

Table 2. **Quantitative comparison with other methods.** With the exception of SampleDepth(PredNet), all comparisons were made using the KITTI Depth Completion validation set, which contains sparse GT.

do. On the other hand, our SampleDepth does not use the RGB image as input, while they do. Keeping this in mind, we use the sparse GT provided by KITTI as the signal to sample from, and report results in Table 2.

We evaluate our method and that of Gofer *et al.* [11] on three sampling rates and observe that SampleDepth (The Lower-bound version) outperforms Gofer *et al.* [11] in all cases. Moreover, even our *fixed* solution, which does not take any prior during inference, and generates only one mask across the entire dataset, is able to achieve similar performance to Gofer *et al.* [11]. *Fixed*-mask performance is slightly better for 4K sampled points, but slightly worse for lower sample rates. Additionally, our method offers a much faster inference time, that can be executed on edge devices. We also report in the table the results of Wolf *et al.* [39] for the lowest sampling ratio of only 1,024 points and observe

that our method outperforms it.

Two other methods, that sample depth maps for depth completion tasks, are not mentioned in the table. The method of Tcenov *et al.* [33] is suitable for sampling only a dense signal. Therefore, their results are reported only on the simulated dataset Synthia *et al.* [29]. Bergman [2] examined only very low sampling rates (fewer than 1000 points).

4.3. Ablation Study

Sampling Ratio Figure 7 presents a comparison between agnostic sampling and SampleDepth for various sampling ratios. In this case, we are sampling from the ground truth depth maps provided in the KITTI dataset. The original GT depth maps consist of approximately 90K points. SampleDepth leads to better depth completion results for all tested sampling ratios, from 19K, all the way down to 2,400 points (which is equivalent to a sampling rate of 1:37)

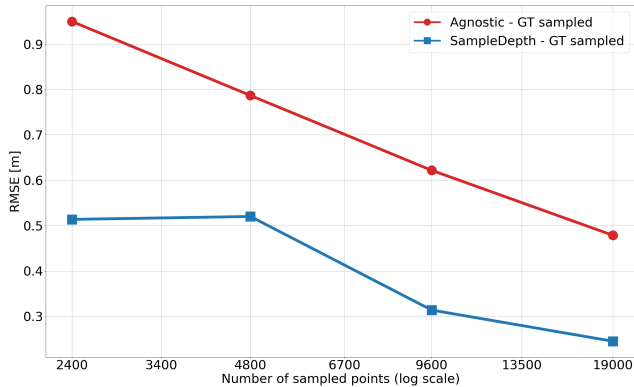


Figure 7. **Depth completion accuracy with SampleDepth.** Regarding the sampling process in this graph, the sampled signal is the prior itself. KITTI Depth Completion selected validation set is used for evaluation.

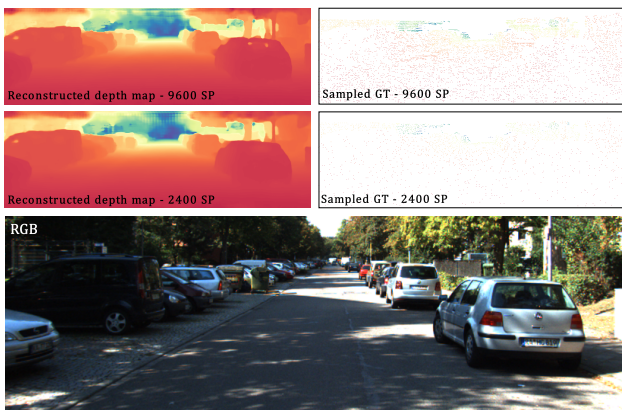


Figure 8. **KITTI GT sampling using SampleDepth.** Two sampled points selected, 2400 and 9600, and sampled using the Lower-bound method. Resulting depth maps from both reconstructions are very similar.

Figure 8 illustrates the quantitative results obtained from sampling the GT signal using SampleDepth for 2,400 and 9,600 points. As can be seen, the completed depth map in both cases is almost indistinguishable. We provide additional results in the supplementary material in which LiDAR signals are being sampled.

Sampling distribution In the quantitative results (Figure 5), we observed that SampleDepth samples more at far away points. We analyzed this observation further and found that this is indeed the case. Figure 9 shows the distribution of depth values at sampled points as collected for both our method and the agnostic approach. SampleDepth has almost twice as many samples at points that are more farther than 85m. Additionally, there is a significant decrease in the number of points that have been sampled within a distance of less than 10m. For the intermediate depth ranges, both methods show indistinguishable distribution trends. A higher percentage of depth samples are taken from 10 – 15m, and the number of sampled points decreases as the depth is increased.

Transferability SampleDepth can be trained with different depth completion networks. In this experiment, we use the depth completion networks proposed by Gansbeke *et al.* [35] and Li *et al.* [19]. Table 3 compares SampleDepth, trained with two different downstream tasks, against the agnostic method. As can be seen, using SampleDepth cuts RMSE error by about 50%, and the MAE by about 25%, compared to the agnostic method, for both downstream tasks.

In fact, it is possible to train SampleDepth using one depth completion network and use it, as is, with another network, as can be seen in Table 4. In the experiments reported in this table, the depth completion network is kept frozen

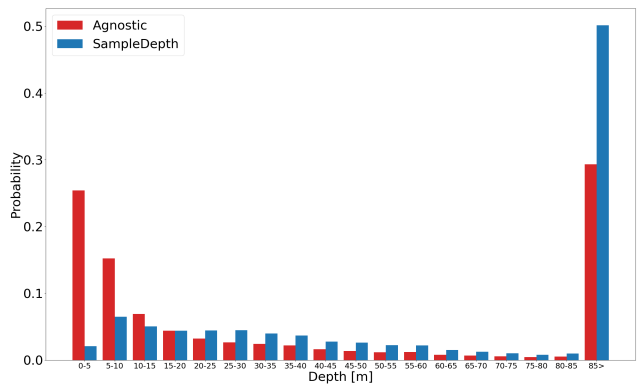


Figure 9. **Sampled depth distribution.** The sample distribution is derived from evaluation of the agnostic and ours methods on the SHIFT validation dataset. SampleDepth refers to our End-to-End adaptive approach.

Downstream network	Agnostic		SampleDepth	
	RMSE	MAE	RMSE	MAE
Gansbeke <i>et al.</i> [35]	0.4785	0.118	0.245	0.097
Li <i>et al.</i> [19]	0.495	0.126	0.254	0.089

Table 3. **A comparison of our solution vs agnostic sampling with two downstream depth completion networks.** Here we use the "Lower bound" sampling method for SampleDepth. The GT depth maps have been sampled to 19K points and have been evaluated on KITTI Depth Completion selected validation set.

Mode	SampleDepth	Downstream task	RMSE	MAE	SP
Regular	Li <i>et al.</i> [19]	Li <i>et al.</i> [19]	0.327	0.113	17.1k
Regular	Gansbeke <i>et al.</i> [35]	Gansbeke <i>et al.</i> [35]	0.301	0.110	13.9k
Mixed&Match	Gansbeke <i>et al.</i> [35]	Li <i>et al.</i> [19]	0.293	0.119	13.9k

Table 4. **Mixed and match.** In the regular mode, the Downstream task is trained using an agnostic sample of 19K points and frozen. Then, SampleDepth is trained while its output is fed into the freeze task network. When using the mixed and match mode, there is no additional training, only evaluation on the pre-trained mixed Samplers and networks. KITTI Depth Completion selected validation set is used for evaluation. SP stand for sampled points.

and only SampleDepth is trained. Observe that in the third row of the table SampleDepth was trained on the network of Gansbeke *et al.* [35] and then combined with the network of Li *et al.* [19] with no further finetuning. The results are nearly indistinguishable from the regular case where we train and test SampleDepth with the same depth completion network (the top two rows in the table).

Prediction-Completion Correlation Figure 10 demonstrate the correlation between the accuracy of predicating the next frame using PredNet, \tilde{D}_t , and the quality of the final reconstructed map \hat{D}_t . As can be seen, the better the accuracy of prediction is, the higher the quality of the reconstructed depth map.

Prediction Accuracy As can be seen in Figure 11, the larger the ego-motion between successive input frames, $\tilde{D}_{t-1:t-b}$, the more difficult it becomes for PredNet to predict the next reconstructed depth map, \tilde{D}_t . The left column contains sequences in which a vehicle containing the camera is stationary and stops at a red light. PredNet is able to predict the dynamic objects in the scene fairly well, such as the two cars. There are two sequences in the middle and right columns with larger ego-motion between frames. Consequently, PredNet is less effective at predicting fine details.

5. Conclusions

We proposed a novel adaptive LiDAR sampling approach, that uses information from previous time steps as

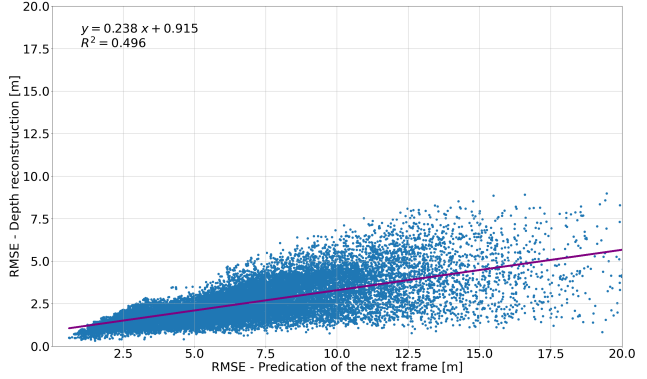


Figure 10. **Prediction-Completion Correlation.** A better prediction of the next frame will result in a higher quality final reconstruction.

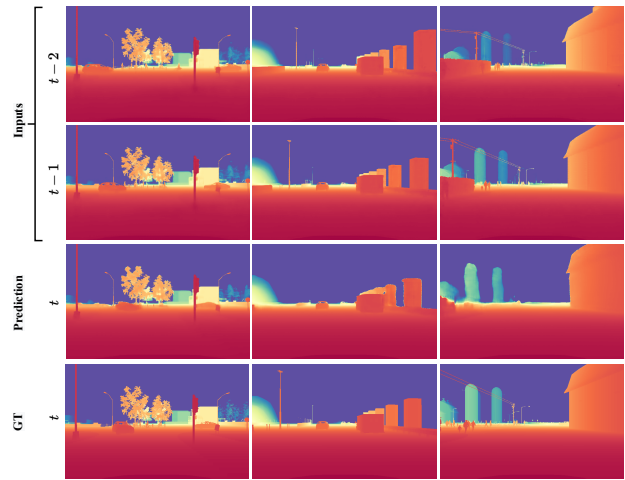


Figure 11. **PredNet prediction of the next frame.** The network gets K past time reconstructed maps and predict the next frame. Left row: the vehicle in the frame is static, while the other objects in the frame are dynamic. Middle row: driving scenario on a highway. Right row: countryside driving

a prior in order to predict the current sampling mask. Our solution is based on SampleDepth, a network that optimizes the sampling mask subject to a downstream depth completion task. The use of temporal data allows us to outperform the agnostic sampling mask that is currently being used. Experiments on two different datasets suggest that our method can reduce depth estimation error by more than 20%, given the adaptive sampling masks computed on the fly by SampleDepth. Moreover, we have shown that SampleDepth can be trained with one depth completion network and transferred, as is and with no fine-tuning, to work with a different depth completion network with indistinguishable impact on performance.

References

- [1] Lin Bai, Yiming Zhao, Mahdi Elhousni, and Xinming Huang. Depthnet: Real-time lidar point cloud depth completion for autonomous vehicles. *IEEE Access*, 8:227825–227833, 2020. [2](#)
- [2] Alexander W Bergman, David B Lindell, and Gordon Wetzstein. Deep adaptive lidar: End-to-end optimization of sampling and depth completion at low sampling rates. In *2020 IEEE International Conference on Computational Photography (ICCP)*, pages 1–11. IEEE, 2020. [2](#), [7](#)
- [3] Xinjing Cheng, Peng Wang, and Ruigang Yang. Learning depth with convolutional spatial propagation network. *IEEE transactions on pattern analysis and machine intelligence*, 42(10):2361–2379, 2019. [2](#)
- [4] Nathaniel Chodosh, Chaoyang Wang, and Simon Lucey. Deep convolutional compressed sensing for lidar depth completion. In *Computer Vision–ACCV 2018: 14th Asian Conference on Computer Vision, Perth, Australia, December 2–6, 2018, Revised Selected Papers, Part I 14*, pages 499–513. Springer, 2019. [2](#)
- [5] Qiqin Dai, Henry Chopp, Emeline Pouyet, Oliver Cossairt, Marc Walton, and Aggelos K Katsaggelos. Adaptive image sampling using deep learning and its application on x-ray fluorescence image reconstruction. *IEEE Transactions on Multimedia*, 22(10):2564–2578, 2019. [3](#)
- [6] Oren Dovrat, Itai Lang, and Shai Avidan. Learning to sample. In *Proceedings of the IEEE/CVF Conference on Computer Vision and Pattern Recognition*, pages 2760–2769, 2019. [2](#)
- [7] Abdelrahman Eldesokey, Michael Felsberg, and Fahad Shahbaz Khan. Propagating confidences through cnns for sparse data regression. *arXiv preprint arXiv:1805.11913*, 2018. [2](#)
- [8] Chelsea Finn, Xin Yu Tan, Yan Duan, Trevor Darrell, Sergey Levine, and Pieter Abbeel. Deep spatial autoencoders for visuomotor learning. In *2016 IEEE International Conference on Robotics and Automation (ICRA)*, pages 512–519. IEEE, 2016. [3](#)
- [9] Zhangyang Gao, Cheng Tan, Lirong Wu, and Stan Z Li. Simvp: Simpler yet better video prediction. In *Proceedings of the IEEE/CVF Conference on Computer Vision and Pattern Recognition*, pages 3170–3180, 2022. [2](#)
- [10] Andreas Geiger, Philip Lenz, and Raquel Urtasun. Are we ready for autonomous driving? the kitti vision benchmark suite. In *2012 IEEE conference on computer vision and pattern recognition*, pages 3354–3361. IEEE, 2012. [4](#)
- [11] Eyal Gofer, Shachar Praisler, and Guy Gilboa. Adaptive lidar sampling and depth completion using ensemble variance. *IEEE Transactions on Image Processing*, 30:8900–8912, 2021. [2](#), [6](#)
- [12] Ross Goroshin, Michael F Mathieu, and Yann LeCun. Learning to linearize under uncertainty. *Advances in neural information processing systems*, 28, 2015. [3](#)
- [13] Kaiming He, Xiangyu Zhang, Shaoqing Ren, and Jian Sun. Delving deep into rectifiers: Surpassing human-level performance on imagenet classification. In *Proceedings of the IEEE international conference on computer vision*, pages 1026–1034, 2015. [5](#)
- [14] Jun-Ting Hsieh, Bingbin Liu, De-An Huang, Li F Fei-Fei, and Juan Carlos Niebles. Learning to decompose and disentangle representations for video prediction. *Advances in neural information processing systems*, 31, 2018. [2](#)
- [15] Huaizu Jiang, Deqing Sun, Varun Jampani, Ming-Hsuan Yang, Erik Learned-Miller, and Jan Kautz. Super slomo: High quality estimation of multiple intermediate frames for video interpolation. In *Proceedings of the IEEE conference on computer vision and pattern recognition*, pages 9000–9008, 2018. [2](#)
- [16] Diederik P Kingma and Jimmy Ba. Adam: A method for stochastic optimization. *arXiv preprint arXiv:1412.6980*, 2014. [11](#)
- [17] Jason Ku, Ali Harakeh, and Steven L Waslander. In defense of classical image processing: Fast depth completion on the cpu. In *2018 15th Conference on Computer and Robot Vision (CRV)*, pages 16–22. IEEE, 2018. [2](#)
- [18] Itai Lang, Asaf Manor, and Shai Avidan. Samplenet: Differentiable point cloud sampling. In *Proceedings of the IEEE/CVF Conference on Computer Vision and Pattern Recognition*, pages 7578–7588, 2020. [2](#)
- [19] Ang Li, Zejian Yuan, Yonggen Ling, Wanchao Chi, Chong Zhang, et al. A multi-scale guided cascade hourglass network for depth completion. In *Proceedings of the IEEE/CVF Winter Conference on Applications of Computer Vision*, pages 32–40, 2020. [1](#), [4](#), [7](#), [8](#)
- [20] Xiaodan Liang, Lisa Lee, Wei Dai, and Eric P Xing. Dual motion gan for future-flow embedded video prediction. In *proceedings of the IEEE international conference on computer vision*, pages 1744–1752, 2017. [2](#)
- [21] Guilin Liu, Kevin Shih, Robert Kirby, Jonathan Barker, David Tarjan, Andrew Tao, Bryan Catanzaro, et al. Video prediction using spatially displaced convolution, Sept. 26 2019. US Patent App. 16/360,853. [2](#)
- [22] Lee-Kang Liu, Stanley H Chan, and Truong Q Nguyen. Depth reconstruction from sparse samples: Representation, algorithm, and sampling. *IEEE Transactions on Image Processing*, 24(6):1983–1996, 2015. [2](#)
- [23] Hengjie Lu, Shugong Xu, and Shan Cao. Sgtbn: Generating dense depth maps from single-line lidar. *IEEE Sensors Journal*, 21(17):19091–19100, 2021. [2](#)
- [24] Fangchang Ma and Sertac Karaman. Sparse-to-dense: Depth prediction from sparse depth samples and a single image. In *2018 IEEE international conference on robotics and automation (ICRA)*, pages 4796–4803. IEEE, 2018. [1](#), [2](#)
- [25] Jinsun Park, Kyungdon Joo, Zhe Hu, Chi-Kuei Liu, and In So Kweon. Non-local spatial propagation network for depth completion. In *European Conference on Computer Vision*, pages 120–136. Springer, 2020. [1](#), [2](#)
- [26] Adam Paszke, Sam Gross, Soumith Chintala, Gregory Chanan, Edward Yang, Zachary DeVito, Zeming Lin, Alban Desmaison, Luca Antiga, and Adam Lerer. Automatic differentiation in pytorch. 2017. [4](#)
- [27] Jiaxiong Qiu, Zhaopeng Cui, Yinda Zhang, Xingdi Zhang, Shuaicheng Liu, Bing Zeng, and Marc Pollefeys. Deeplidar: Deep surface normal guided depth prediction for outdoor scene from sparse lidar data and single color image. In

- Proceedings of the IEEE/CVF Conference on Computer Vision and Pattern Recognition*, pages 3313–3322, 2019. [2](#)
- [28] Olaf Ronneberger, Philipp Fischer, and Thomas Brox. U-net: Convolutional networks for biomedical image segmentation. In *International Conference on Medical image computing and computer-assisted intervention*, pages 234–241. Springer, 2015. [2](#), [3](#)
- [29] German Ros, Laura Sellart, Joanna Materzynska, David Vazquez, and Antonio M Lopez. The synthia dataset: A large collection of synthetic images for semantic segmentation of urban scenes. In *Proceedings of the IEEE conference on computer vision and pattern recognition*, pages 3234–3243, 2016. [7](#)
- [30] Nitish Srivastava, Elman Mansimov, and Ruslan Salakhudinov. Unsupervised learning of video representations using lstms. In *International conference on machine learning*, pages 843–852. PMLR, 2015. [2](#)
- [31] Tao Sun, Mattia Segu, Janis Postels, Yuxuan Wang, Luc Van Gool, Bernt Schiele, Federico Tombari, and Fisher Yu. Shift: A synthetic driving dataset for continuous multi-task domain adaptation. In *Proceedings of the IEEE/CVF Conference on Computer Vision and Pattern Recognition*, pages 21371–21382, 2022. [4](#)
- [32] Kensuke Taguchi, Shogo Morita, Yusuke Hayashi, Wataru Imaeda, and Hironobu Fujiyoshi. Uncertainty-aware interactive lidar sampling for deep depth completion. In *Proceedings of the IEEE/CVF Winter Conference on Applications of Computer Vision*, pages 3028–3036, 2023. [2](#)
- [33] Ilya Tcenov and Guy Gilboa. How to guide adaptive depth sampling? *arXiv preprint arXiv:2205.10202*, 2022. [2](#), [7](#)
- [34] Jonas Uhrig, Nick Schneider, Lukas Schneider, Uwe Franke, Thomas Brox, and Andreas Geiger. Sparsity invariant cnns. In *2017 international conference on 3D Vision (3DV)*, pages 11–20. IEEE, 2017. [2](#), [4](#)
- [35] Wouter Van Gansbeke, Davy Neven, Bert De Brabandere, and Luc Van Gool. Sparse and noisy lidar completion with rgb guidance and uncertainty. In *2019 16th international conference on machine vision applications (MVA)*, pages 1–6. IEEE, 2019. [1](#), [2](#), [4](#), [7](#), [8](#), [11](#), [12](#)
- [36] Ruben Villegas, Jimei Yang, Seunghoon Hong, Xunyu Lin, and Honglak Lee. Decomposing motion and content for natural video sequence prediction. *arXiv preprint arXiv:1706.08033*, 2017. [2](#)
- [37] Ruben Villegas, Jimei Yang, Yuliang Zou, Sungryull Sohn, Xunyu Lin, and Honglak Lee. Learning to generate long-term future via hierarchical prediction. In *international conference on machine learning*, pages 3560–3569. PMLR, 2017. [2](#)
- [38] Yunbo Wang, Haixu Wu, Jianjin Zhang, Zhifeng Gao, Jianmin Wang, S Yu Philip, and Mingsheng Long. Predrnn: A recurrent neural network for spatiotemporal predictive learning. *IEEE Transactions on Pattern Analysis and Machine Intelligence*, 45(2):2208–2225, 2022. [2](#)
- [39] Adam Wolff, Shachar Praisler, Ilya Tcenov, and Guy Gilboa. Super-pixel sampler: a data-driven approach for depth sampling and reconstruction. In *2020 IEEE International Conference on Robotics and Automation (ICRA)*, pages 2588–2594. IEEE, 2020. [2](#), [6](#)

Supplementary

A. Additional results

LiDAR signal sampling. Certain scenarios, such as memory management or communication, may benefit from the sampling of signals that have already been sampled. This type of application can also be addressed by our SampleDepth solution.

For this purpose, we sample the LiDAR signal from the KITTI depth completion dataset, while the LiDAR also serves as a prior.

As shown in Figure 12, SampleDepth outperforms agnostic sampling for any number of sample points. Figure 13 illustrates the quantitative results obtained from sampling 12.5% from the LiDAR signal. As can be seen, the depth map generated by the raw LiDAR data is almost identical to the one produced by SampleDepth.

B. Ablation study

B.1. ImplicitPred

In Table 5, our adaptive solution ImplicitPred is evaluated with different number of past frames, neural network capacity, and regularization. The best performance obtained with deeper U-Net architecture, include $L_{sampledMaps}$ loss and using 2 past frame.

B.2. PredNet

In subsection 4.3 we already demonstrated the correlation between the accuracy of predicating the next frame using PredNet, \tilde{D}_t , and the quality of the final reconstructed map \hat{D}_t .

Based on Table 6, it can be seen that using four previous frames optimizes the quality of PredNet prediction of the next frame. A greater number of past frames are not tested due to computational limitations.

C. Experimental settings

The details of the experiments are presented in Table 7. Adam [16] optimizer is used for all experiments. Considering that the table hyper-parameters refer to 19K sampled points, it should be possible to work with lower sample ratios.

The basic training regime of SampleDepth consists of three steps: First, a depth completion task is pre-trained independently (ID's: a, d, g, j) according to Gansbeke *et al.* [35] training regime. Differences between experiments for this stage primarily arise from the depth inputs to the depth completion network. As an example, in the Lower-bound method for 19K sampled points, ID (a), the task network will train while sampling GT in an agnostic manner to 19K points.

Then, the task network weights are freeze, and SampleDepth is trained while it's output feed into the frozen task network (ID's: b, e, h, k, t).

Finally, the task network and SampleDepth are fine-tuned together (ID's: c, f, i, l).

There are some experiments in which weights from other stages are utilized, in order to bypass the three stages. The depth completion task and SampleDepth are loaded with pre-trained weights and have just been fine-tuned.

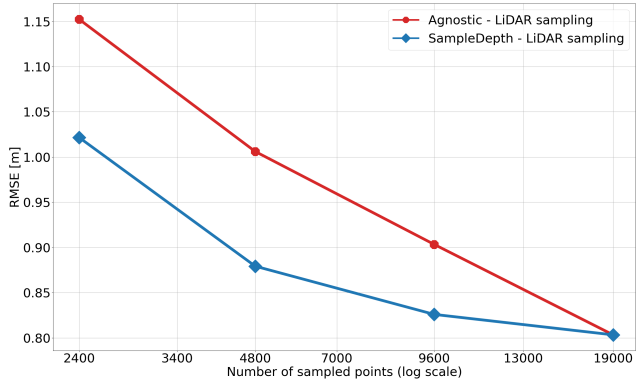


Figure 12. **LiDAR sampling** Regarding the sampling process in this graph, the sampled signal is the prior itself. KITTI Depth Completion selected validation set is used for evaluation.

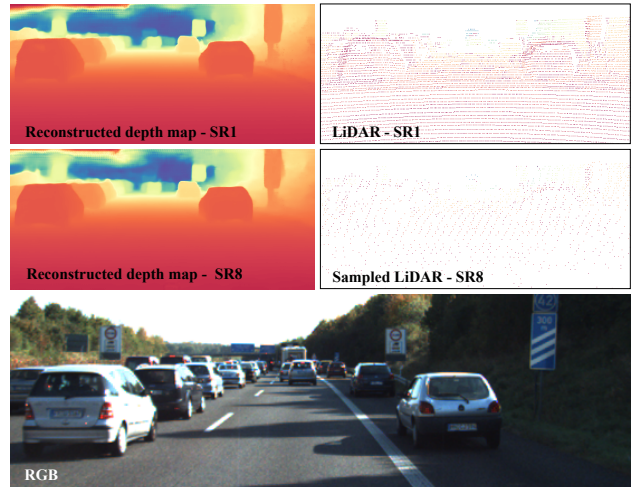


Figure 13. **KITTI LiDAR Sampling using SampleDepth.** SampleDepth selects 12.5% of the points from the raw LiDAR. The reconstructed depth maps of SR1 and SR8 are very similar.

Architecture	L_{task}	L_{sample}	$L_{SampledMaps}$	1 past frames	2 past frames	3 past frames
U-Net(4 levels)	✓	✓		2.536	2.645	2.896
U-Net(5 levels)	✓	✓	✓	2.551	2.525	2.542

Table 5. **ImplicitPred performance as function of architecture, regularization and number of last frames.** The results reported in RMSE[m] for the final reconstructed depth map. This evaluation was conducted on the SHIFT dataset. The "level" refer to the number of contraction layers.

Architecture	2 past frames	3 past frames	4 past frames
U-Net(5 levels)	6.845	6.742	6.552

Table 6. **PredNet performance as function of inputs number of last frames.** The results reported in RMSE[m] for the explicit predication of the next frame. The SHIFT dataset was used for this evaluation.

Experiment	Dataset	ID	Task network	SampleDepth	Epochs	Batch size	LR	α	Load weights
Lower bound	KITTI	(a)	Trained	-	30	18	0.001	-	*erfnet[35]
		(b)	Freeze	Trained	20	8	0.0001	4	(a)
		(c)	Trained	Trained	7	10	0.001	50	(b)
	KITTI Pseudo GT	(d)	Trained	-	30	20	0.002	-	*erfnet[35]
		(e)	Freeze	Trained	20	8	0.0001	25	(d)
		(f)	Trained	Trained	10	8	0.0001	50	(e)
	SHIFT	(g)	Trained	-	30	20	0.008	-	*erfnet[35]
		(h)	Freeze	Trained	20	10	0.0001	50	(g)
		(i)	Trained	Trained	7	10	0.001	100	(h)
LiDAR	KITTI	(j)	Trained	-	30	18	0.001	-	*erfnet[35]
		(k)	Freeze	Trained	20	8	0.0001	4	(j)
		(l)	Trained	Trained	7	10	0.001	50	(k)
Fixed Mask	KITTI	(m)	Trained	Trained	30	1	0.1	50	(c)
	KITTI Pseudo GT	(n)	Trained	Trained	30	1	0.0001	5	(f)
	SHIFT	(o)	Trained	Trained	30	1	0.001	20	(i)
PredNet (Only predication of next frame)	Pseudo GT KITTI	(p)	-	-	30	10	0.0002	-	-
	SHIFT	(q)	-	-	30	10	0.001	-	-
SampleDepth (PredNet prior)	Pseudo GT KITTI	(r)	Trained	Trained	30	10	0.0001	25	(f)
	SHIFT	(s)	Trained	Trained	30	10	0.001	100	(i)
ImplicitPred	SHIFT	(t)	Freeze	Trained	30	8	0.0001	100	(i)

Table 7. **Hyperparameters.** The table provides information on the hyperparameters values used for training SampleDepth at each stage and method.